

Growth in multi-component alloys: Theoretical and numerical determination of phase concentrations

Arka Lahiri, T.A.Abinandanan, Abhik Choudhury, M.S. Bhaskar

Department of Materials Engineering, Indian Institute of Science, 560012 Bangalore, India

Understanding the role of solute diffusivities in equilibrium tie-line selection during growth of a second phase in ternary and higher multicomponent two phase alloys is an important problem due to the strong dependence of mechanical properties on compositions. In this paper, we derive analytical expressions for predicting tie-lines and composition profiles in the matrix during growth of planar and cylindrical precipitates with the assumption of diagonal diffusivity matrices. We confirm our calculations by sharp interface and phase field simulations. The numerical techniques are in turn utilized for investigating the role of off-diagonal entries in the diffusivity matrix. In addition, the sharp interface methods allow for the tracking of the tie-line compositions during growth of 2D precipitates which contribute to an understanding of the change in equilibrium tie-lines chosen by the system during growth.

PACS numbers: 64.70.D-, 81.30.Fb, 81.30.-t

Keywords: Multicomponent, ternary, phase-field, sharp-interface, growth, diffusion

I. INTRODUCTION

Properties of phases are closely related to their chemical compositions. In this respect, prediction of phase compositions during growth often becomes important with regards to the choice of alloy compositions and processing conditions. Theoretical understanding of the problem of diffusion controlled growth of phases from a super-saturated matrix in binary systems, is mainly due to the developments presented in [1–3]. While in binary alloys, the compositions of the phases are most of the time determined directly from the phase diagram and the imposed temperature history, for ternary and higher multi-component alloys this becomes non-trivial as the two-phase equilibria is not unique. A consequence of this is seen experimentally in Fe-C-Mo alloys [4], and other Fe-C-X systems [5, 6] (where X stands for the substitutional alloying elements such as, Mn [7, 8], Ni [9], Cr [10]) where the growth of a particular second-phase (ferrite) from the matrix (austenite) occurs in the absence of any partition of the element X, which has very low diffusivity. This phenomenon, which is also sometimes referred to as ‘paraequilibrium’, is a direct consequence of the existence of multiple equilibria between the two-phases which is absent in binary alloys. More pertinently, the choice of the equilibria can be shown to depend on the diffusivity of the different species as has already been shown in a classical theoretical analysis by Coates et al. [11, 12], where the conjugate problem of computing the bulk alloy compositions under different diffusivity matrices, for which a given tie-line is selected, is addressed. Another theoretical contribution by Bourne et al. [13] derives expressions for composition profiles in the matrix along with predictions for equilibrium compositions. The method in [13] is an indirect one, where the diffusivities are solved for by iterating over the possible tie-line compositions, whereby a prior knowledge of the equations of coexistence lines along with that of the tie-lines in the system is required.

This motivates our study in this paper which has three principal aims. Firstly, we derive an analytical theory for diagonal diffusivity matrices (for both cylindrical and planar geometries), following previous work in [11, 12] and [13], that not only allows a direct calculation of the quantities of interest (tie-lines and composition fields in the matrix) for a given bulk alloy composition and diffusivity matrix, but also incorporates the Gibbs-Thomson correction of phase equilibria in 2D systems. To this end, we have employed nothing more than the basic thermodynamic information associated with the variation of the free-energies of the phases with compositions, which differentiates it from the previous approaches by presenting a more elegant way of prediction of tie-lines given the bulk alloy composition and a diffusivity matrix which is easily extensible to an alloy system with any number of components.

Secondly, a particular multi-component phase field model formulation based on a grand-potential formalism [14, 15] is employed to study growth. The model itself has the possibility to incorporate information from thermodynamic databases in an effective manner [16], which will allow its subsequent utilization for study of growth in real systems. The phase field results are compared with both the analytical model and an independent sharp interface (front tracking) numerical model, the objective being the validation of this particular formulation for use in subsequent work involving growth of multiple phases in complicated geometries. In addition, the phase field and the sharp interface models are compared against each other for diffusivity matrices comprising of off-diagonal entries, where an analytical treatment is difficult. To our knowledge, although phase field models have been used for multi-component studies (Ti-Al-V [17], Al-Si-Cu-Fe [18], Al-Si-Cu-Mg-Ni [19], Mg-Al-Mn [20], Ni-Al-Cr-Ta-W [21], Al-Si-Cu-Fe-Mg-Mn-Ni-Zn [22], Fe-C-B [23]), the influence of diffusivity matrices on the choice of equilibria has not been dealt in detail. For example in [24], the authors do investigate the particular case of

‘para-equilibrium’ in the case of an Fe-C-Mn alloy, however, the simulations are not directed towards deriving the phase compositions in the relevant scaling regime during growth.

Thirdly, as a result of the comparison of the different methods and the investigation of the dependence of the phase equilibria on the diffusivity/mobility matrices we highlight the need for their accurate measurement, without which the implications of understanding derived from numerical simulations, such as the phase field method, become unreliable.

We begin our discussion with planar growth in Section II where a theoretical analysis for the case of diagonal diffusivities in the scaling regime is presented in Section IIA, followed by a description of the numerical simulation methods. The sharp interface (front tracking model) is described in Section IIB and phase field (diffuse interface mode) in Section IIC (that is generic for all dimensions), which utilize the thermodynamics of a representative alloy system elaborated in Section IID. Subsequently, we present the comparison between the analysis and the simulations for planar growth in Section IIE. Thereafter, radial growth is analyzed in Section III, with the theoretical development in Section IIIA and the description of the corresponding numerical sharp-interface model for radial growth in Section IIIB, followed by the comparison of the composition profiles in the matrix between analysis and simulation methods in Section IIIC. We end with a discussion in Section IV and conclusions and outlook in Section V.

II. PLANAR GROWTH

In this section, we develop an analytical theory and conduct sharp interface and phase field simulations to understand the problem of tie-line selection during planar growth of a multicomponent alloy.

A. Theory

In the theoretical analysis, we are going to consider the situation where we have a 1D domain, with one-sided diffusivity, i.e. only the matrix has non-zero diffusion coefficients. Additionally, we will restrict our theoretical discussion to diagonal diffusivities. Furthermore, to ensure brevity, we express all the equations in the vector-matrix notation, where $\{\cdot\}$ represents a vector and $[\cdot]$ represents a matrix. We start with the following governing equations in the matrix which write as,

$$\left\{\frac{\partial c_i}{\partial t}\right\} = [D_{ij}] \left\{\frac{\partial^2 c_j}{\partial x^2}\right\}, \quad (1)$$

where, both the indices i and j iterate over all the $(K - 1)$ solute components in a K component system.

The Stefan boundary condition at the interface writes as,

$$v \left\{c_{i,eq}^\alpha - c_{i,eq}^\beta\right\} = -[D_{ij}] \left\{\frac{\partial c_j}{\partial x}\right\} \bigg|_{x_f}, \quad (2)$$

with $c_{i,eq}^{\alpha,\beta}$ as the equilibrium compositions at the interface for the matrix (α) and the precipitate (β) and v being the velocity of the interface with its position being denoted by x_f .

Here, we restrict ourselves to the situation corresponding to independent solute diffusion and perform a co-ordinate transformation, writing $\eta = x/\sqrt{t}$. In these co-ordinates the governing equations transform to,

$$\left\{\frac{\partial^2 c_i}{\partial \eta^2}\right\} = \frac{-\eta}{2} \left\{\frac{1}{D_{ii}} \frac{\partial c_i}{\partial \eta}\right\}, \quad (3)$$

while the Stefan-boundary condition at the interface reads,

$$\left\{\frac{\partial c_i}{\partial \eta}\right\} \bigg|_{\eta_s} = \frac{-\eta_s}{2} \left\{\frac{\Delta c_i}{D_{ii}}\right\}, \quad (4)$$

where $\eta_s = x_f/\sqrt{t}$ is the corresponding value at the interface, which is at a position x_f at a given time t . We have used, $\Delta c_i = (c_{i,eq}^\alpha - c_{i,eq}^\beta)$.

Integrating the Eq. 3 once, we derive,

$$\left\{\frac{\partial c_i}{\partial \eta}\right\} = \left\{\lambda_i \exp\left(\frac{-\eta^2}{4D_{ii}}\right)\right\}, \quad (5)$$

where λ_i 's are integration constants. Using the Stefan's conditions in Eq. 4, the value of the integration constants can be derived as,

$$\{\lambda_i\} = \frac{-\eta_s}{2} \left\{\frac{\Delta c_i}{D_{ii} \exp\left(\frac{-\eta_s^2}{4D_{ii}}\right)}\right\}, \quad (6)$$

where, since λ_i 's are independent of η , the value of η_s must be a constant for the given alloy composition.

Integrating the Eq. 5 once again and invoking the boundary condition that the far-field compositions corresponding to $\eta = \infty$ are known as $\{c_i^\infty\}$ and the compositions at the interface $\eta = \eta_s$ are the equilibrium compositions $\{c_{i,eq}^\alpha\}$, we derive,

$$\left\{\frac{c_i^\infty - c_{i,eq}^\alpha}{\int_{\eta_s}^\infty \exp\left(\frac{-\eta^2}{4D_{ii}}\right) d\eta}\right\} = \frac{-\eta_s}{2} \left\{\frac{\Delta c_i}{D_{ii} \exp\left(\frac{-\eta_s^2}{4D_{ii}}\right)}\right\}, \quad (7)$$

which can be reduced using the complement of the error functions as,

$$\{c_i^\infty - c_{i,eq}^\alpha\} = -\frac{\sqrt{\pi}\eta_s}{2} \left\{ \frac{\Delta c_i \operatorname{erfc}\left(\frac{\eta_s}{2\sqrt{D_{ii}}}\right)}{\sqrt{D_{ii}} \exp\left(\frac{-\eta_s^2}{4D_{ii}}\right)} \right\}, \quad (8)$$

In the following, we apply the above analysis for a three component system where B, C are the solutes, and the values $c_{B,eq}^\alpha, c_{C,eq}^\alpha$ refer to the equilibrium compositions of the two components in the matrix phase at the interface. Eq. 8 can be utilized in two ways, the first is to derive all the alloy compositions c_B^∞ and c_C^∞ , that can have a given tie-line one of whose ends is given by the matrix composition at the interface, which is highlighted in Fig. 1. One can see that for the situation where D_{BB}/D_{CC} is unity, the corresponding tie-lines for all values of η_s , are equal to the thermodynamic tie-line containing the alloy composition. With change in the ratio of D_{BB}/D_{CC} , the alloy compositions start to shift from the thermodynamic tie-line and the graph portrays all the possibilities which are derived through variation of the value of η_s , each for a different ratio of D_{BB}/D_{CC} .

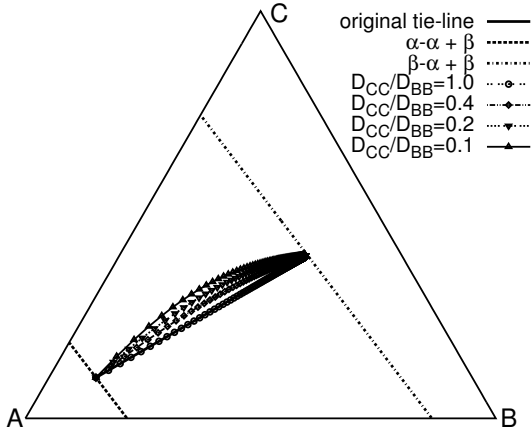


Figure 1. Loci of alloy compositions which give the same tie-line given by the equilibrium matrix (α) compositions (c_B, c_C) as (0.1, 0.1) and precipitate (β) composition (0.4, 0.4) for different diffusivity ratios D_{CC}/D_{BB} .

The second possibility is to derive the equilibrium compositions $c_{B,eq}^\alpha$ and $c_{C,eq}^\alpha$, and the value of η_s using Eq. 8, given the bulk alloy composition c_B^∞ and c_C^∞ and the diffusivity matrix. This however requires that we know the functional relationships $c_B(\mu_B, \mu_C)$ and $c_C(\mu_B, \mu_C)$ and also the relationship between $\mu_{B,eq}(\mu_{C,eq})$ which is a property of the thermodynamic co-existence line. Using them, the two equations in (8) can be reduced to a system of two equations containing $\mu_{C,eq}$ and η_s , which can then be consistently solved for. The resulting $\mu_{C,eq}$ can then be utilized to fix $\mu_{B,eq}$ using the equilibrium thermodynamics of the co-existence line and thereby the

matrix compositions $c_B^\alpha(\mu_B, \mu_C), c_C^\alpha(\mu_B, \mu_C)$. Further, the precipitate compositions can also be fixed using the corresponding relations for $c_B^\beta(\mu_B, \mu_C), c_C^\beta(\mu_B, \mu_C)$. For a linearized phase diagram we delineate the different possible tie-lines for each of the bulk alloy compositions for a single diffusivity ratio D_{BB}/D_{CC} in Fig. 2.

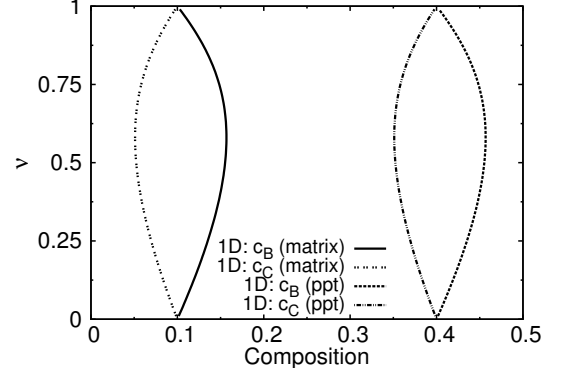


Figure 2. Combination of tie-line equilibrium compositions (c_B, c_C) for the matrix and the precipitate corresponding to different alloy compositions along the tie-line (0.1, 0.1) (matrix) (0.4, 0.4) (precipitate) compositions, for a ratio of diffusivity $D_{CC}/D_{BB} = 0.1$. The thermodynamic information about co-existence lines is derived from Eq. 22. The parameter ν signifies a point corresponding to the choice along this tie-line; $\nu = 0$ represents an alloy composition equal to the matrix (α) while $\nu = 1$ for an alloy composition equal to that of the precipitate (β).

The composition profile for a given η_s and far-field composition can be derived simply by using the Eq. 8 as,

$$\{c_i(\eta)\} = \left\{ c_i^\infty - (c_i^\infty - c_{i,eq}^\alpha) \frac{\operatorname{erfc}\left(\frac{\eta}{2\sqrt{D_{ii}}}\right)}{\operatorname{erfc}\left(\frac{\eta_s}{2\sqrt{D_{ii}}}\right)} \right\}, \quad (9)$$

where $\eta = x/\sqrt{t}$ is the variable in the transformed co-ordinate system, for all $x > x_f$ and time t , x_f being the position of the interface.

In the following two subsections, we describe two numerical simulation models namely, a front-tracking (sharp interface) model and a diffuse interface (phase field) model, for treating the transient evolution of the interface under a general condition of arbitrary diffusivity matrices.

B. Sharp interface model

The governing Eq. 1 can be solved numerically along with the boundary condition at the interface given by Eq. 2 using an advective scheme where the motion of the interface is accounted for by an equal and opposite advective term which brings the interface back to its origin

place (this is a numerically effective way of treating the front tracking problem as the interface cell remains invariant). Thereby, the interface stays stationary in this frame of reference. The modified governing equations in the vector-matrix notation are written as,

$$\left\{ \frac{\partial c_i}{\partial t} - v \frac{\partial c_i}{\partial x} \right\} = [D_{ij}] \left\{ \frac{\partial^2 c_j}{\partial x^2} \right\}, \quad (10)$$

where v is the instantaneous local velocity of the interface. The position of the interface is marked by the interface cell, where the equilibrium compositions of the precipitate and the matrix are specified. For a ternary system with B and C as solutes, the gradients $\partial c_{B,C}/\partial x$ are written in discrete form using these compositions at the interface cell and the bulk compositions on the matrix side, next to the interface. To compute the interfacial compositions, the pair of equations in (2) are self-consistently solved for both the velocity and the equilibrium chemical potentials $\mu_{B,eq}, \mu_{C,eq}$ at the interface. This requires that the composition functions $c_{B,C}^{\alpha,\beta}(\mu_B, \mu_C)$ are known from thermodynamics along with the equilibrium relation between the two chemical potentials, $\mu_{B,eq}(\mu_{C,eq})$.

Using these, the pair of equations in (2), can be transformed such that the unknowns are the equilibrium chemical potential of a given component ($\mu_{C,eq}$) and the velocity (v). Once the chemical potential $\mu_{C,eq}$ is known, the other chemical potential $\mu_{B,eq}$ can also be fixed using the thermodynamic relation between them and thereby also the individual phase compositions at the interface, $c_{B,C}^{\alpha,\beta}(\mu_B, \mu_C)$. The compositions are then utilized to compute the gradients in the governing equations in Eq. 10 and thereby evolve the compositions $c_{B,C}$ in the matrix phase through one time-step, using also the velocity that is derived from the Stefan condition. When the scaling regime is reached, the equilibrium compositions at the interface reach a steady state. The corresponding composition profiles can then be compared with the theoretical analysis in the preceding section. This method, gives a fast accurate benchmark in 1D, in comparison to the more computationally intensive method to be discussed in the following section.

C. Phase field model

In this subsection, we give a brief description of phase field (diffuse interface) model, also described in [14, 25], for studying growth in multi-component systems. All the equations are presented in the tensorial form and so they describe the model regardless of the dimensionality considered. Phase evolution is determined by the phenomenological minimization of the grand canonical

density functional (Ω) written as,

$$\Omega(\boldsymbol{\mu}, T, \phi) = \int_V \left[\Psi(\boldsymbol{\mu}, T, \phi) + \left(\epsilon a(\phi, \nabla \phi) + \frac{1}{\epsilon} w(\phi) \right) \right] dV, \quad (11)$$

where ϵ is the length scale related to the diffuse interface, and ϕ is the order parameter determining the presence of the precipitate phase, i.e., regions where $\phi = 1$, demarcate the precipitate, and $\phi = 0$, the matrix. The functional $a(\phi, \nabla \phi)$ is the gradient energy written as $\sigma |\nabla \phi|^2$, σ being numerically equal to the interfacial energy. Functional $w(\phi)$ is a surface potential density written as a double-well function of the order-parameter ϕ , which is $9\sigma\phi^2(1-\phi)^2$. We write the grand potential density Ψ as an interpolation of the individual grand potential densities Ψ^α, Ψ^β , each of which are functions of the diffusion potential vector $\boldsymbol{\mu} = \{\mu_1, \dots, \mu_{K-1}\}$ containing the $K-1$ independent diffusion potentials and temperature T in the system as,

$$\Psi(\boldsymbol{\mu}, T, \phi) = \Psi^\alpha(\boldsymbol{\mu}, T) h(1-\phi) + \Psi^\beta(\boldsymbol{\mu}, T) h(\phi) \quad (12)$$

$h(\phi)$ is the interpolation polynomial written as $h(\phi) = \phi^2(3-2\phi)$, which ensures that $h(\phi) + h(1-\phi) = 1$. The phase concentration expressions can be derived in terms of the diffusion potential, using the relation,

$$c_i^{\alpha,\beta}(\boldsymbol{\mu}, T) = -V_m \frac{\partial \Psi^{\alpha,\beta}(\boldsymbol{\mu}, T)}{\partial \mu_i}, \quad (13)$$

where V_m is the molar volume which is considered equal for all the components in this entire paper. Thereafter, the equations of motion for the phase field and the composition variables are derived in a standard manner.

The evolution equations for the phase field ϕ can be derived as,

$$\tau_{\alpha\beta}\epsilon \frac{\partial \phi}{\partial t} = \epsilon \left(\nabla \cdot \frac{\partial a(\phi, \nabla \phi)}{\partial \nabla \phi} \right) - \frac{1}{\epsilon} \frac{\partial w(\phi)}{\partial \phi} - \frac{\partial \Psi(\boldsymbol{\mu}, T, \phi)}{\partial \phi}, \quad (14)$$

where, the relaxation constants for the matrix-precipitate interfaces $\tau_{\alpha\beta}$, are calculated for pure diffusion-controlled regime using the analysis described in [14].

For a general multi-phase, multi-component system, the evolution equations for the components of the diffusion potential $\boldsymbol{\mu}$ can be expressed in vector-matrix form by,

$$\left\{ \frac{\partial \mu_i}{\partial t} \right\} = \left[\sum_{p=\alpha,\beta} h_p(\phi) \frac{\partial c_i^p(\boldsymbol{\mu}, T)}{\partial \mu_j} \right]_{ij}^{-1} \left\{ \nabla \cdot \sum_{j=1}^K M_{ij}(\phi) \nabla \mu_j - \sum_{p=\alpha,\beta} c_i^p(\boldsymbol{\mu}, T) \frac{\partial h_p(\phi)}{\partial t} \right\}. \quad (15)$$

where $\{\cdot\}$ represents a vector of dimension $(K-1)$ while $[\cdot]$ denotes a matrix of dimension $(K-1) \times (K-1)$. For conciseness, we have utilized expressions $h_\alpha(\phi) = h(1-\phi)$ and $h_\beta(\phi) = h(\phi)$. Here, $M_{ij}(\phi)$ is the atomic mobility, where the individual phase mobilities are interpolated as,

$$M_{ij}(\phi) = M_{ij}^\alpha(1-\phi) + M_{ij}^\beta\phi. \quad (16)$$

Each of the $M_{ij}^{\alpha,\beta}$ is defined using the expression,

$$[M_{ij}^{\alpha,\beta}] = [D_{ik}^{\alpha,\beta}] \left[\frac{\partial c_k^{\alpha,\beta}(\mu, T)}{\partial \mu_j} \right], \quad (17)$$

where D_{ij}^α and D_{ij}^β are the solute inter-diffusivities in α and β respectively.

For the simulations in the present section, we will impose diffusivities only in one of the phases (matrix phase, α), which implies the diffusivity matrix is zero for the precipitate phase, β . The anomalous artificial solute trapping that is known to arise because of this choice is countered by using a multi-component version of the anti-trapping current that is derived in [14]. This is an additional flux in the diffusion equation which acts towards the matrix phase.

D. Thermodynamics: Equilibrium across a planar front

The driving forces for a phase transformation from α to β is the difference between the grand-potential densities of the phases, i.e., $\Delta\Psi = \Psi^\alpha - \Psi^\beta$. In this section we utilize a linearized phase diagram around the compositions of interest, which also allows for a simple coupling to thermodynamic databases. The driving force, $\Delta\Psi$ is derived by linearly expanding the individual grand-potential densities in terms of the departure of the diffusion potential from a given equilibrium value $\mu_{eq}^* = \{\mu_{i,eq}^*\}$ as,

$$\Psi^{\alpha,\beta}(\mu, T) = \Psi^{\alpha,\beta}(\mu_{eq}^*, T) + \left\{ \frac{\partial \Psi^{\alpha,\beta}}{\partial \mu_i} \right\}_{\mu_{i,eq}^*} \{\mu_i - \mu_{i,eq}^*\} \quad (18)$$

and therefore, the leading order term in the driving force for the phase transformation α to β writes as,

$$\begin{aligned} \Delta\Psi^{\alpha\beta} &= (\Psi^\alpha - \Psi^\beta) \\ &= \left\{ \frac{\partial \Psi^\alpha}{\partial \mu_i} - \frac{\partial \Psi^\beta}{\partial \mu_i} \right\}_{\mu_{i,eq}^*} \{\mu_i - \mu_{i,eq}^*\}, \end{aligned} \quad (19)$$

where, we have used the vector-matrix notation. Using the thermodynamic relationship in Eq. 13, we can equivalently write the preceding equation as,

$$\Delta\Psi^{\alpha\beta} = \frac{1}{V_m} \left\{ c_{i,eq}^{\beta,*} - c_{i,eq}^{\alpha,*} \right\} \{\mu_i - \mu_{i,eq}^*\}. \quad (20)$$

The phase compositions as a function of the chemical potential are thereafter linearly extrapolated from the chosen equilibrium points $\{c_{i,eq}^*\}$ as,

$$\{c_i^{\alpha,\beta}\} = \{c_{i,eq}^{\alpha,\beta}\}^* + \left[\frac{\partial c_i^{\alpha,\beta}}{\partial \mu_j} \right]_{\mu_{j,eq}^*} \{\mu_j - \mu_{j,eq}^*\}, \quad (21)$$

which are utilized in the evolution equation of the components as described in Eq. 15. The susceptibility matrix $\left[\frac{\partial c_i^{\alpha,\beta}}{\partial \mu_j} \right]_{\mu_{j,eq}^*}$ which is also used in the construction of the

atomic mobility matrix in Eq. 17 is a term that can be also retrieved from the thermodynamic databases. The equilibrium composition vectors $\{c_{eq}^{\alpha,\beta}\}^*$ of the phases are used in constructing a linearized expansion of the driving force, as given in Eq. 20 and eventually in the evolution equation of the order-parameter given in Eq. 14 (all quantities which are denoted with a superscript $*$, pertain to values around which the linearization is performed). [26]

Using the approximate driving forces as the leading order term in the expansion of the grand-potential densities, also fixes the relation between the diffusion potentials of the different components along the co-existence lines, which is derived by setting, $\Delta\Psi^{\alpha\beta} = 0$ in Eq.20. For the case of a ternary alloy, this relation reads,

$$\frac{\mu_{B,eq} - \mu_{B,eq}^*}{c_{C,eq}^{\alpha,*} - c_{C,eq}^{\beta,*}} = - \frac{\mu_{C,eq} - \mu_{C,eq}^*}{c_{B,eq}^{\alpha,*} - c_{B,eq}^{\beta,*}} \quad (22)$$

i.e, the set of equilibrium diffusion potentials of the components are related to each other using the previous relation. The equilibrium phase co-existence lines can also be derived after some algebraic manipulation as,

$$\frac{c_{B,eq}^{\alpha,\beta} - (c_{B,eq}^{\alpha,\beta})^*}{c_{C,eq}^{\alpha,\beta} - (c_{C,eq}^{\alpha,\beta})^*} = \frac{\left(\frac{\partial c_B^{\alpha,\beta}}{\partial \mu_C} - \frac{1}{\rho} \frac{\partial c_B^{\alpha,\beta}}{\partial \mu_B} \right)^*}{\left(\frac{\partial c_C^{\alpha,\beta}}{\partial \mu_C} - \frac{1}{\rho} \frac{\partial c_C^{\alpha,\beta}}{\partial \mu_B} \right)^*}, \quad (23)$$

where $\rho = (c_{B,eq}^{\alpha,*} - c_{B,eq}^{\beta,*}) / (c_{C,eq}^{\alpha,*} - c_{C,eq}^{\beta,*})$. Therefore, given a set of equilibrium compositions $c_{B,eq}^{\alpha,*}, c_{C,eq}^{\alpha,*}, c_{B,eq}^{\beta,*}, c_{C,eq}^{\beta,*}$, and the corresponding susceptibility $\left[\frac{\partial c_i^{\alpha,\beta}}{\partial \mu_j} \right]_{\mu_{j,eq}^*}$, which are two quantities that

can be derived from thermodynamic databases, the equilibrium co-existence lines in the vicinity of the chosen compositions are correctly represented for the given system of interest. The susceptibility matrix can

be easily determined by computing the inverse of the matrix, $\left[\frac{\partial \mu_i^{\alpha, \beta}}{\partial c_j} \right]_{(c_j^{\alpha, \beta})^*}$, which can be retrieved from the derivatives of the free-energy expressions in the databases near the compositions of interest. Fig. 3 sketches the approximate scheme that is used and the resulting co-existence lines corresponding to the expressions in Eq. 23.

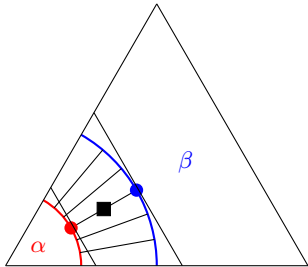


Figure 3. Two-phase equilibrium in a ternary alloy. The phase-coexistence lines at a given temperature are drawn as solid curves and the corresponding tie-lines are drawn as solid black lines between the co-nodes on the co-existence curves. For a particular alloy composition indicated by the solid square, the susceptibility matrix is computed corresponding to the compositions of the phases comprising the tie-line, which are marked here by solid circles and which are also the composition vectors $c_{eq}^{\alpha,*}$, $c_{eq}^{\beta,*}$ that are used in the approximation. The tangents to the co-existence tie-lines are the local extrapolations corresponding to the these thermodynamic properties of the alloy at the respective phase compositions.

E. Results

Having described the analytical theory and the numerical techniques that will be employed to understand precipitate growth in a ternary alloy in 1D, we begin this section by comparing predictions of composition profiles from phase field, sharp interface and analytical expression against each other[27]. In this regard, it's important to note that all our calculations are performed in the non-dimensional setting. The definitions of the relevant scales that can be used to convert dimensionless quantities into dimensional values for a particular system are presented in the Appendix.

1. Three-way comparison between analytical theory and simulation methods

We firstly depict a comparison between the compositions derived from phase field computations and the theoretical predictions for the case of the diffusivity matrix being an identity matrix. Fig. 4(a) highlights the excellent agreement between theory and the phase field

computations, where the analytical predictions are superposed on the phase field computations by matching the interface positions in the analysis and the phase field methods.

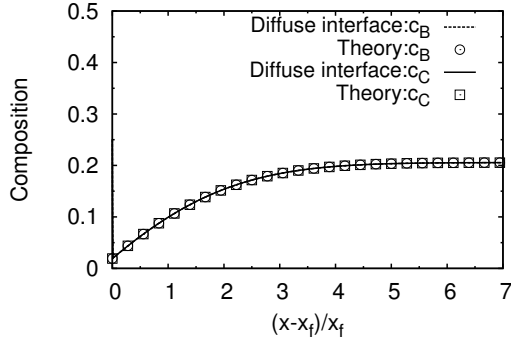
As a second benchmark we choose an alloy composition from the theoretical analysis in Fig. 1, which does not alter the interfacial compositions of the two phases for $D_{BB} \neq D_{CC}$. Fig. 4(b), highlights the comparison between the composition profiles obtained from sharp interface and phase field computations. The value of η_s from the sharp interface (0.625), phase field (0.637) and the theoretical analysis (0.628), confirm the excellent agreement, between the three methods.

As a third benchmark, we also simulated the influence of the presence of off-diagonal elements in the diffusivity matrix. The results are depicted in Fig. 4(c), which again show a good agreement between the sharp interface and the phase field methods. For an arbitrary alloy composition along the loci of alloy compositions in Fig. 1, for $D_{CC}/D_{BB} = 0.1$ ($D_{CC} = 0.1$), the tie-line compositions as seen from the simulations, no longer remain invariant, as $c_{B,eq}^{\alpha}$ and $c_{C,eq}^{\alpha}$ are not equal, contrary to the property of the chosen thermodynamic tie-line. Additionally, the profile of c_B shows a behavior which is different from the case of pure diagonal diffusivities with a shallower increase ($\partial c_B / \partial x = 0$ at the interface) of the compositions near the interface. The non-existence of the composition gradients at the interface of the component with a larger diffusivity is explained later.

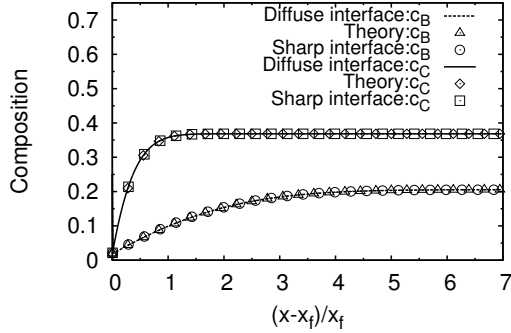
Subsequently, we have chosen a far-field composition along a given thermodynamic tie-line, and let the simulations from the sharp interface and phase field methods select the tie-line compositions during growth. This is the inverse question, and more relevant to gaining a control of processing conditions, where one can predict the precipitate and matrix compositions given a particular alloy composition. For the case of the diagonal diffusivities, these tie-line compositions can also be predicted analytically as has been previously described in Fig. 2. We have superposed the predictions from the sharp interface simulations on this figure and find excellent agreement between the theoretical and the numerical method as shown in Fig. 5.

An exemplary comparison of the composition profiles from the sharp interface and the phase field profiles, is depicted in Fig. 6(a), for independent diffusion of solutes but for unequal diffusivities.

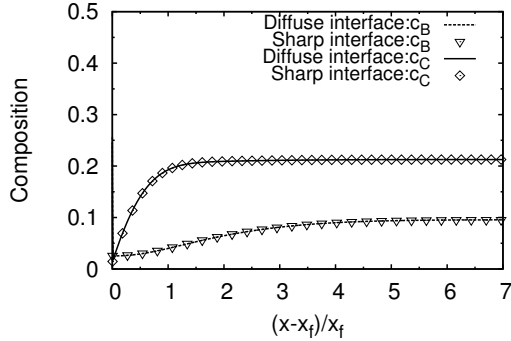
Following this, we have repeated the computations with off-diagonal components in the diffusivity matrix as reported in Fig. 6(b). Here, from both the sharp interface and the phase field computations, we confirm that the selected tie-line compositions are similar for both the pure diagonal diffusivities and diffusivity matrices with off-diagonal terms (as also seen in Fig. 5).



(a)



(b)



(c)

Figure 4. Composition profiles at a total time of 200000 with the far-field matrix (α) compositions and the diffusivity matrix components being: (a) $c_B = 0.205$ and $c_C = 0.205$; $D = I$ (identity matrix), (b) $c_B = 0.205$ and $c_C = 0.368$; $D_{BB} = 1.0$ and $D_{CC} = 0.1$ with the off-diagonal terms set to zero, and (c) $c_B = 0.095$ and $c_C = 0.212$; $D_{BB} = 1.0$ and $D_{CC} = D_{BC} = D_{CB} = 0.1$. The thermodynamic tie-line compositions were $c_{B,eq}^\beta = c_{C,eq}^\beta = 0.481$ and $c_{B,eq}^\alpha = c_{C,eq}^\alpha = 0.019$. The phase field simulation box was of size 2000 with $dx = 1.0$ and $dt = 0.01$. The $\partial c / \partial \mu$ matrix was taken to be equal for both the phases and is stated in the Appendix red along with the values of σ and ϵ that are used in all phase field computations.

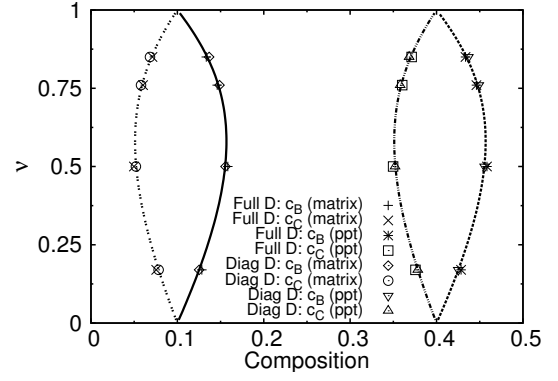
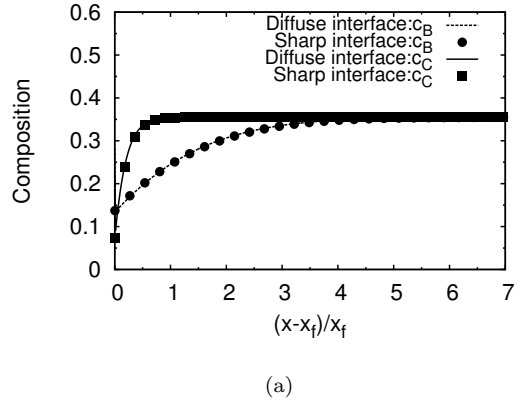
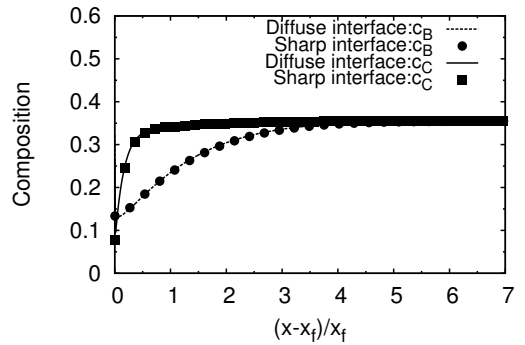


Figure 5. Tie lines predicted from sharp interface simulations in 1D are compared against theoretical predictions. The diagonal diffusivity matrix (“Diag D” in the figure legend) considered has components $D_{BB} = 1.0$, $D_{CC} = 0.1$ with the off-diagonal elements set to zero. The full diffusivity matrix (“Full D” in the figure legend) has components $D_{BB} = 1.0$, $D_{CC} = D_{BC} = D_{CB} = 0.1$. The theoretical predictions are depicted by the same continuous lines as done in Fig. 2.



(a)



(b)

Figure 6. Composition profiles at a total time of 300000 with the far-field matrix (α) compositions and the diffusivity matrix components being: (a) $c_B = 0.355$ and $c_C = 0.355$; $D_{BB} = 1.0$ and $D_{CC} = 0.1$ with the off-diagonal terms set to zero, and (b) $c_B = 0.355$ and $c_C = 0.355$; $D_{BB} = 1.0$ and $D_{CC} = D_{BC} = D_{CB} = 0.1$. The other simulation parameters are the same as in Fig. 4.

2. Diffusion distances

The diffusion length scales of the different components during growth have a profound impact on the kinetics of the system. For example, the relative influence of the components on the coarsening rates can be derived from the information related to the impingement of the composition profiles which are related to the diffusion lengths. Similarly, the relative sensitivity of the interface towards diffusional instabilities can also be linked to the diffusional lengths of the components. In a ternary system, this particular measure of the diffusion length scales of the different components can be obtained by considering the ratio of composition gradients at the interface. This can be derived from the Stefan conditions stated in Eq. 2 as,

$$\left\{ \frac{\partial c_i}{\partial x} \right\} \bigg|_{x_f} = -v [D_{ij}^{-1}] \{ \Delta c_j \}. \quad (24)$$

From Eq. 24 we can derive $(\partial c_B / \partial x) / (\partial c_C / \partial x)$ which is the ratio of the inverses of the relative diffusion lengths of the components B and C . Thus, once the tie-line compositions (Δc_B and Δc_C) are fixed, the ratio of the diffusion length can also be predicted from the preceding relation. Applying Eq. 24 on the system depicted in Fig. 6(a), the interfacial gradients are found to be 0.000489 and 0.00489 in c_B and c_C respectively. This calculation is in excellent agreement to the interfacial gradients obtained from the sharp interface simulations (in phase field calculations, the diffuseness of the interface makes the determination of the tie-line compositions through extrapolations of the bulk composition profiles, a little difficult). The relative diffusion lengths (that of c_B to c_C), as given by the ratio of the inverses of the interfacial gradients calculates to 10 indicating that the component B diffuses over a distance that is 10 times over that of C . The same analysis when applied to the system in Fig. 6(b), yields $\partial c_B / \partial x = 0$ and $\partial c_C / \partial x = 0.0054975$ at the interface (also confirmed by sharp interface calculations). The non-existence of an interfacial gradient in c_B reflects on the dominating influence of the slower diffusing species on the growth dynamics and that the diffusion of B is instantaneous compared to that of C and thereby the diffusivity of C principally determines the diffusion kinetics.

3. Effective diffusivity: Independent solute diffusion

A quantity which might be of interest for interpretation of the diffusion length scales is that of the effective diffusivity (D_{AA}^{eff}) which is a composite diffusivity characterizing the α - β transformation. The combined diffusion of the components B and C can be mapped to a diffusion in the solvent A whose diffusivity (anointed as the effective diffusivity (D_{AA}^{eff})) turns out to be a weighted average

Table I. Effective diffusivities of alloys having 40% supersaturation on two different tie-lines (these tie-lines are used for fitting the thermodynamics). Alloys on tie-line 2 are leaner in C

tie-line	Δc_B	Δc_C	D_{AA}^{eff}
1	-0.546	-0.312	0.234
2	-0.679	0.178	0.348

of the diffusivities of the solutes. With the the diffusion of components B and C occurring independently, adding the Stefan conditions in Eq. 2 gives:

$$v \left(\frac{\Delta c_B}{D_{BB}} + \frac{\Delta c_C}{D_{CC}} \right) = \frac{\partial c_A}{\partial x} \bigg|_{x_f} = -v \frac{\Delta c_A}{D_{AA}^{eff}}, \quad (25)$$

which leads to the expression:

$$D_{AA}^{eff} = - \left(\frac{1}{D_{BB}} \frac{\Delta c_B}{\Delta c_A} + \frac{1}{D_{CC}} \frac{\Delta c_C}{\Delta c_A} \right)^{-1}. \quad (26)$$

Thus, the effective diffusivity expressed in Eq. 26 is a function of not only the individual inter-diffusivities of the components but also of the chosen tie-line compositions ($c_{B,eq}^\alpha = c_{C,eq}^\alpha = 0.1$ and $c_{B,eq}^\beta = c_{C,eq}^\beta = 0.4$) As a consequence of the inverse interpolation, the effective diffusivity will have a value closer to the diffusivity of the slower moving species. Eq. 26 predicts $D_{AA}^{eff} = 1.0$ for a system having a diagonal diffusivity matrix with $D_{BB} = D_{CC} = 1.0$. The situation here is actually equivalent to the case of a binary alloy with A as the diffusing species and the equilibrium compositions of the precipitate and the matrix being given by the tie-line compositions in the ternary alloy ($1 - c_B - c_C$).

For a system with $D_{BB} = 1.0$ and $D_{CC} = 0.1$ and $D_{BC} = D_{CB} = 0$ (see Fig. 6(a)), D_{AA}^{eff} becomes 0.182, for which such a binary mapping does not hold. The influence of the choice of the particular tie-line on the effective diffusivity is also depicted in the Table I, where two different values of effective diffusivity are calculated based on two different tie-lines with the same given supersaturation. Please note that the Δc_A and Δc_B are the equilibrium composition values that the system chooses at the interface.

4. Effective diffusivity: Coupled solute diffusion

For a system displaying coupled diffusion of the solutes, the gradients at the interface can be calculated from Eq. 24 and (D_{AA}^{eff}) can be computed as:

$$\frac{\partial c_B}{\partial x} \bigg|_{x_f} + \frac{\partial c_C}{\partial x} \bigg|_{x_f} = - \frac{\partial c_A}{\partial x} \bigg|_{x_f} = v \frac{\Delta c_A}{D_{AA}^{eff}}, \quad (27)$$

which leads to:

$$D_{AA}^{eff} = \frac{v\Delta c_A}{\left. \frac{\partial c_B}{\partial x} \right|_{x_f} + \left. \frac{\partial c_C}{\partial x} \right|_{x_f}} = \frac{-\Delta c_A (D_{BB}D_{CC} - D_{BC}^2)}{(D_{CC} - D_{BC})\Delta c_B + (D_{BB} - D_{BC})\Delta c_C}, \quad (28)$$

where we have imposed $D_{BC} = D_{CB}$. For a system with $D_{BB} = 1.0$, $D_{CC} = 0.1$, $D_{BC} = D_{CB} = 0.1$ (see Fig. 6(b)), the effective diffusivity was calculated to be 0.2.

Thus, through our study in 1D, we have been able to predict the new equilibrium phase compositions selected during growth. Furthermore, strategies for computing the solute diffusion distances in the matrix are also discussed. Though, this information is critical to an understanding of the microstructural length scale selection during growth, it must be complemented by an analysis of the role played by capillarity in dimensions greater than one. This leads us to take up the same problem again, but in 2D.

III. RADIAL GROWTH OF A CYLINDRICAL PRECIPITATE

The subject of interest is dealt in a manner similar to planar growth study. An analytical theory is developed followed by a description of the sharp interface technique in 2D. The phase field model has already been explained in conjunction with the 1D problem and is not discussed here. The description of the system thermodynamics is modified to account for the effect of curvature.

A. Theory

In the radial coordinate system, the governing differential equations are written in the vector-matrix form as,

$$\left\{ \frac{\partial c_i}{\partial t} \right\} = \frac{1}{r} [D_{ij}] \left\{ \frac{\partial}{\partial r} \left(r \frac{\partial c_j}{\partial r} \right) \right\}. \quad (29)$$

The Stefan boundary condition at the interface ($r = R$) in the radial coordinate system is the same as in Eq. 2 with r in place of x .

Restricting ourselves to diagonal diffusivities, a coordinate transformation of Eq. 29 to express them as functions of $\eta = r/\sqrt{t}$ followed by an integration with respect to η leads to,

$$\left\{ \frac{\partial c_i}{\partial \eta} \right\} = \left\{ \frac{\lambda_i^R}{\eta} \exp \left(\frac{-\eta^2}{4D_{ii}} \right) \right\}, \quad (30)$$

where λ_i^R 's are integration constants. Using the Stefan's conditions in Eq. 4, the value of the integration constants can be derived as,

$$\{\lambda_i^R\} = \frac{-\eta_s^2}{2} \left\{ \frac{\Delta c_i(R)}{D_{ii} \exp \left(\frac{-\eta_s^2}{4D_{ii}} \right)} \right\}, \quad (31)$$

where $\eta_s = R/\sqrt{t}$ is the corresponding value at the interface, which is at a position R at a given time t and the definition of Δc_i remain the same as in 1D, except that now they are functions also of the radius of the precipitate through the Gibbs-Thomson effect, i.e the compositions $c_{i,eq}^{\alpha,\beta}$ are functions of the radius of the precipitate.

Far into the growth regime, the composition differences Δc_i , vary very slowly upon change of radius, therefore can be treated as constants and since λ_i^R are constants independent of η the only possibility is that η_s be a constant, for such a scaling regime to exist.

Integrating Eq. 30 from η_s to ∞ , we can derive using Eq. 31,

$$\left\{ \frac{c_i^\infty - c_{i,eq}^\alpha(R)}{\int_{\eta_s}^\infty \frac{1}{\eta} \exp \left(\frac{-\eta^2}{4D_{ii}} \right) d\eta} \right\} = \frac{-\eta_s^2}{2} \left\{ \frac{\Delta c_i(R)}{D_{ii} \exp \left(\frac{-\eta_s^2}{4D_{ii}} \right)} \right\}, \quad (32)$$

Particularizing Eq. 32 to ternary systems, we can see that while in the 1D case, employing the functions $c_B^{\alpha,\beta}(\mu_B, \mu_C)$, $c_C^{\alpha,\beta}(\mu_B, \mu_C)$ and $\mu_{B,eq}(\mu_{C,eq})$, yields a system of non-linear equations which can be solved for μ_C and η_s , leading to the equilibrium tie-line compositions, however, for the case of the cylindrical precipitate this is no longer possible. This is because, though the system selects a particular value of η_s during the scaling regime of precipitate growth, it can correspond to a larger R at a later time or a smaller R at an earlier time. This makes it impossible to determine the value of the equilibrium compositions at the interface without the knowledge of the radius R .

Despite this constraint, we can still attempt to understand the effect of dimensionality by ignoring the curvature effect on compositions. Under this assumption, Eq. 32 are solved for μ_C and η_s , leading to curves in Fig. 7, where the growth coefficient is derived for compositions along a given thermodynamic tie-line with diagonal diffusivity matrices described in the Fig. 7. Correspondingly, one can also predict the selected tie-line compositions similar to the computations for case of planar growth as in Fig.2.

However, if the equilibrium compositions at the interface $c_{B,eq}^\alpha, c_{C,eq}^\alpha$ are known, then Eq. 32 can be utilized for generating the composition profiles in the matrix phase α . At any particular instant of time, all η 's which are $> \eta_s$ can be mapped to locations ahead of the interface (i.e., inside the matrix by using $r = \eta\sqrt{t}$) with $c_B(\eta)$ and $c_C(\eta)$ being the compositions at those locations. Integrating Eq. 30 from any particular $\eta(> \eta_s)$ to ∞ , we can derive using Eq. 31,

C. Results

$$\left\{ \frac{c_i^\infty - c_{i,eq}^\alpha(R)}{c_i^\infty - c_i(\eta)} \right\} = \{Q_i\} = \left\{ \frac{\int_{\eta_s}^\infty \frac{1}{\eta} \exp\left(-\frac{\eta^2}{4D_{ii}}\right) d\eta}{\int_{\eta_s}^\infty \frac{1}{\eta} \exp\left(-\frac{\eta^2}{4D_{ii}}\right) d\eta} \right\}, \quad (33)$$

where Q_i 's are constants representing ratios of integrals. Eq. 33 can be re-written to obtain $c_B(\eta)$ and $c_C(\eta)$:

$$\{c_i(\eta)\} = \left\{ \frac{c_{i,eq}^\alpha(R)}{Q_i} + \left(1 - \frac{1}{Q_i}\right) c_i(\infty) \right\}, \quad (34)$$

and this can be done for all $\eta > \eta_s$ to get the composition profiles in the matrix.

B. Sharp-interface model

Eq. 29 can be numerically solved for by discretizing them in a frame attached to the interface as was done for the 1D case. The governing equations can be re-written in the matrix-vector notation for a moving frame of reference as:

$$\left\{ \frac{\partial c_i}{\partial t} - v \frac{\partial c_i}{\partial r} \right\} = [D_{ij}] \left\{ \left(\frac{1}{r} \frac{\partial c_j}{\partial r} + \frac{\partial^2 c_j}{\partial r^2} \right) \right\}, \quad (35)$$

where v is the velocity of the interface at a particular instant of time. Similar to the situation in 1D, this requires the determination of the interfacial compositions at each time step, which are solved by utilizing the Stefan conditions along with the conditions for local thermodynamic equilibrium. In contrast to the situation in 1D where thermodynamic equilibrium is derived by setting the driving force to zero, in 2D, the same is derived by equating the driving force due to phase transformation with that due to curvature, i.e., $\Delta\Psi^{\alpha\beta} = \sigma\kappa$, that reads,

$$\frac{1}{V_m} \left\{ c_{i,eq}^{\beta,*} - c_{i,eq}^{\alpha,*} \right\} \left\{ \mu_i - \mu_{i,eq}^* \right\} = \sigma\kappa, \quad (36)$$

where σ denotes the interfacial energy and κ the curvature which can be approximated by $1/R$ for a cylindrical precipitate. The expression in Eq. 36 can be re-written for a ternary alloy to obtain an expression relating the two diffusion potentials μ_B and μ_C for the case of two independent components as,

$$\mu_B - \mu_{B,eq}^* = \frac{\sigma\kappa V_m}{(c_{B,eq}^{\beta,*} - c_{B,eq}^{\alpha,*})} - \frac{(c_{C,eq}^{\beta,*} - c_{C,eq}^{\alpha,*})(\mu_C - \mu_{C,eq}^*)}{(c_{B,eq}^{\beta,*} - c_{B,eq}^{\alpha,*})}. \quad (37)$$

Using this relation and the relations $c_i^\alpha(\mu)$ one can reduce the Stefan boundary conditions at the interface purely as functions of one of the diffusion potentials and solve for μ_C and the velocity in a manner similar to the situation in 1D [28].

The implication of considering the correction in the local equilibrium due to curvature can be understood by first solving for η_s from Eq. 32 ignoring the influence of curvature on the shift of compositions, for different supersaturations defined by ν , super-imposed with points computed from values obtained from sharp interface computations in 2D incorporating capillarity. The variation in η_s against ν (whose definition is described in the caption to Fig. 2) thus calculated is studied in the context of similar variations obtained from solving the 1D problem (see Fig. 7). Though, we do not address the 3D problem in this study, a variation of η_s with ν for a growth of a spherical particle is also presented in Fig. 7 for the sake of completion.

We see that differences between the analytical predictions without consideration of capillarity and sharp interface computations including capillarity occur for the case where $D_{BB} \neq D_{CC}$ at large volume fractions, while for smaller values of ν , the deviations are small. This implies, that the selection of the growth coefficient η_s is only weakly influenced by capillarity.

Further, phase field and sharp interface numerical simulations both incorporating the influence of capillarity are utilized for deriving the composition profiles far into the scaling regime. These profiles are compared with analytical predictions obtained by solving Eq. 34, where we set the values of equilibrium compositions at the interface, $c_{B,eq}^\alpha$ and $c_{C,eq}^\alpha$ and η_s from sharp interface calculations. Fig. 9 shows the transient evolution of the interfacial compositions obtained from the numerical sharp interface simulations. In Fig. 8(a), the diffusivity matrix is diagonal and the individual diffusivities are set to unity. Here, the composition profiles from the three techniques mentioned above are in excellent agreement with each other. The values of η_s selected by the system is 1.42(1.51) as obtained from phase field (sharp interface) simulations. The changing interface curvature of a growing precipitate sets the interfacial compositions (under local thermodynamic equilibrium) along an extension to the original tie-line only and the system does not select a tie-line with a different c_B/c_C ratio (see Fig. 9(a), where $c_B = c_C$ is the original tie-line).

Focussing on the composition profiles for the case of $D_{BB}/D_{CC} = 10$ ($D_{CC} = 0.1$), we can see from Fig. 8(b), that the interfacial compositions in the matrix do not correspond to the original tie-line where $c_B/c_C = 1.0$. This can also be observed from both the analytically calculated curves (neglecting Gibbs-Thomson) and the data points obtained from sharp interface calculations, for a particular value of ν as seen in Fig. 9(b).

In addition, as expected, the deviations, of tie-line compositions obtained using numerical simulations (considering capillarity), from analytical predictions without incorporating capillarity, reduce with time as the ratio of the radius of the precipitate with respect to the cap-

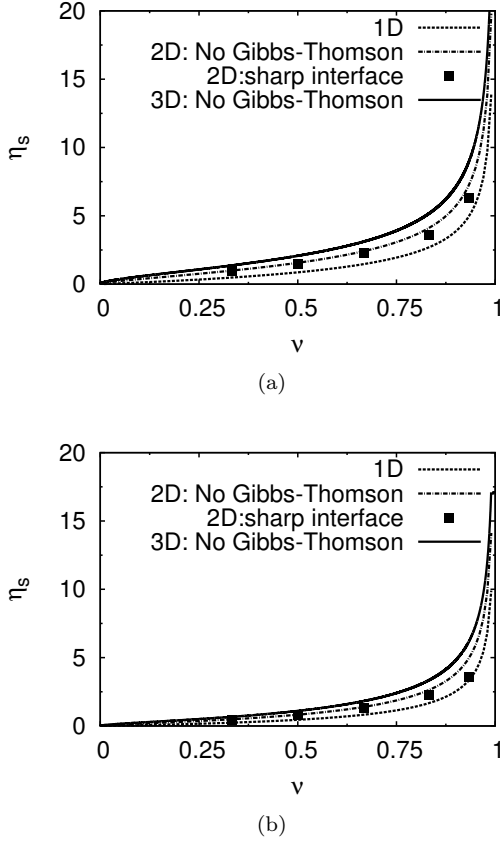


Figure 7. Variation in η_s with ν , for a 2D system with Gibbs-Thomson correction from sharp interface calculations, for (a) $D_{BB} = 1.0$ and $D_{CC} = 1.0$, and (b) $D_{BB} = 1.0$ and $D_{CC} = 0.1$. The other terms in the diffusivity matrix are zero. The results are presented in the context of similar variations obtained for 1D as well as for 2D and 3D systems neglecting the influence of capillarity.

illary length (approximately scaling as: $\left(\frac{\sigma V_m}{(d\mu/dc) \Delta c}\right)$) becomes larger as seen in Fig.9.

The lowered gradients in c_B in Fig. 8(b) at the interface translates to a diffusion distance large enough to interact with the system boundaries. This can explain the slight difference between the sharp interface (also theoretical) and the phase field profiles of component B. More elaborately, the differences arise because it is difficult to impose equivalent boundary conditions between a radial co-ordinate system that is used for both the sharp interface and the theoretical calculations (which agree well) and a cartesian co-ordinate system in a rectangular domain that is used for the phase field. This difference causes a small error for the diffusion profiles with shallower gradients, possibly due to the different interaction with the boundaries in the two co-ordinate systems. The c_C profiles (displaying larger gradients at the interface) obtained from the different schemes described above are in very good agreement with each other as can be seen from Fig. 8(b). Both numerical schemes (phase field and

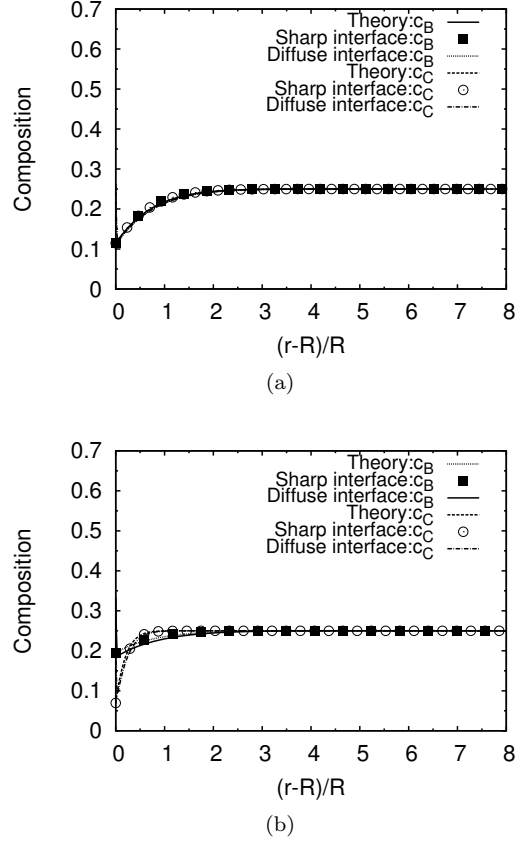


Figure 8. Composition profiles at a $t=10000$ with the far-field liquid compositions being $c_B = 0.25$ and $c_C = 0.25$. The diffusivity matrix is the same as an identity matrix in (a), while it is $D_{BB} = 1.0$ and $D_{CC} = 0.1$ with the off-diagonal entries zero for (b). The simulation is performed on an 800×800 box with $dx = dy = 1.0$, $dt = 0.01$, with the same maintained for sharp interface calculations as well.

sharp interface) predicted the same value of $\eta_s = 0.72$ for this system. The improved match in the η_s 's from the phase field and the sharp interface calculations in this situation compared to the one where $D_{BB}/D_{CC} = 1$ can be attributed to the fact that in the former, the slower diffusing species controls the growth of the precipitate (which happens at a much slower rate than in the case where $D_{CC} = 1$).

Taking cue from the minor changes observed in tie-line selection due to the presence of off-diagonal terms in the diffusivity matrix in 1D, we restrict our studies in 2D to diagonal diffusivity matrices only, knowing that the sharp interface and phase field simulations can be easily extended to capture the dynamics corresponding to a diffusivity matrix with off-diagonal entries.

IV. SUMMARY AND DISCUSSION

In summary, we use numerical simulation methods (phase field, sharp interface) and analytical calcula-

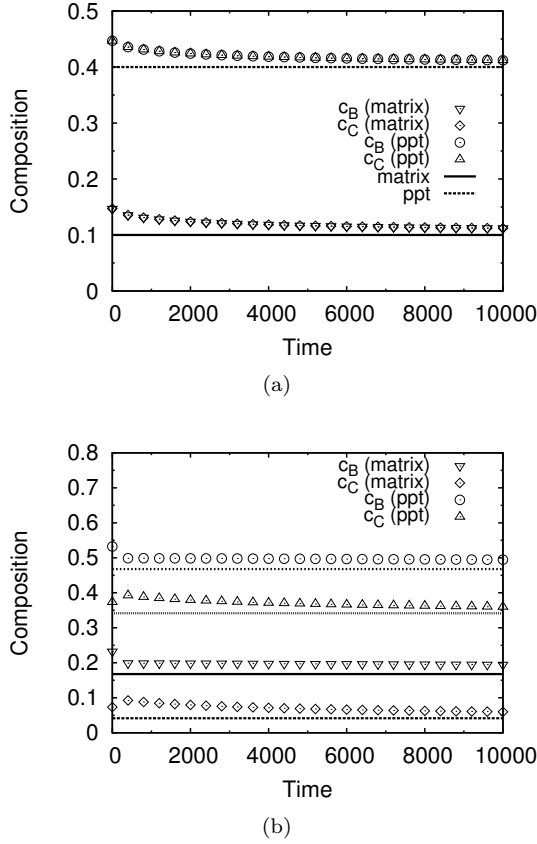


Figure 9. Variation of tie-line compositions with time, with the non-zero diffusivity components being, (a) $D_{BB} = D_{CC} = 1$, and (b) $D_{BB} = 1$, $D_{CC} = D_{BC} = D_{CB} = 0.1$, during radial growth of a precipitate. The lines plotted along side the data-points refer to the analytical calculations without incorporation of capillarity. (time is plotted in non-dimensional units)

tions for the determination of phase equilibria in multi-component systems. Here, firstly we give a prescription for the growth of planar interfaces, where starting from the thermodynamics of the system in terms of the free-energies near the co-existence compositions it is possible to analytically derive not only the tie-line compositions that the phases will select for a given ratio of diffusivities in a diagonal diffusivity matrix but also the range of alloy compositions sharing the same given tie-lines. These predictions agree well against numerical phase field and sharp interface calculations. Additionally, numerical computations have been utilized to extend the study to include the case of full diffusivity matrices which are difficult to treat analytically.

Thereafter, we investigate the growth of cylindrical precipitates in 2D, where our analytical and sharp-interface calculations allow the equilibrium compositions of the phases to vary with curvature. This allows us to capture the continuous selection of different tie-lines during growth of precipitates for different diffusivity ratios. Here as well, the composition profiles obtained from

our theory, sharp interface and phase field calculations agree well with each other at any given instant of time. The influence of the incorporation of the Gibbs-Thomson can be seen in Fig. 7(b), where the deviations of the growth coefficient obtained from sharp interface simulations, from the predictions without the consideration of the Gibbs-Thomson corrections occur at very high volume fractions. Consequently, we can derive that the differences in the predictions of the phase equilibria (with and without Gibbs-Thomson correction in 2D) seem to influence the growth coefficient η_s only weakly at low volume fractions.

The diffusion distances in the matrix for different solutes are also computed which are critical to the prediction of the onset of coarsening. Considering the large magnitude of the diffusion length scales calculated in this paper, they appear to be a quantity easily obscured in experimental studies of multi-particle precipitation where the inter-particle distance is not large enough to resolve the steady-state growth regime from coarsening. Thus, unless experiments are designed specifically to measure diffusion distances during growth, analytical and numerical techniques discussed in this paper provide the only methodologies for computing this important parameter. Furthermore, an effective diffusivity, defined as an average of the individual solute diffusivities weighted by the tie-line compositions is used to represent the overall kinetics of the system.

It is important to highlight at this point that the $\partial c / \partial \mu$ matrix plays an important role in the selection of tie-lines with different c_B / c_C ratios with time. For a precipitate phase which is an intermetallic (very limited solubility around its stoichiometric composition), the components of the $\partial c / \partial \mu$ matrix are expected to be very small in magnitude, resulting in negligible migration of the tie-lines to other c_B / c_C ratios during growth. Analytical and numerical techniques proposed in this paper can help delineate the bulk alloy compositions that ensures growth of such phases with the desired composition. This information can facilitate a stringent control during processing to achieve the microstructural objectives. Additionally, it is noteworthy that the simple scheme of incorporating the thermodynamics for (both phase field and sharp interface methods) is similar to previous work [16] where parabolic free-energy extrapolations are used, while for the present paper, we restrict ourselves to linearized driving forces. The simplicity of the framework allows for easy extension to multicomponent alloys for more than three components and incorporation of information from thermodynamic databases. However, the accuracy of the assumption of linearization, must be checked depending on the deviations of phase equilibria from those around which the linearization is performed.

V. CONCLUSION AND OUTLOOK

To conclude we have the following inferences from the work

- A particular phase field model based on a grand-potential formulation is validated for simulating phase transformations in multicomponent systems, thus setting up the modeling of more complicated kinetic processes such as coarsening and growth in multi-phase systems which are beyond the purview of sharp interface and analytical considerations.
- Analytical approaches for diagonal diffusivity matrices are outlined which allow for the determination of the phase equilibria using the same thermodynamic information also utilized in the phase field simulations, i.e., the information relating to the properties of the free-energies of the respective phases with composition.
- A strong implication of the work is the need for accurate measurements/determination of diffusivity/mobility matrices without which results from numerical simulations become less useful in the quantitative understanding of growth in multicomponent systems.

A corollary that can be derived of the present work is highlighting the important difference between binary alloys and ternary (and higher) systems: Most growth relations for interfaces (interface response functions) relate the velocity of the interface for different morphologies such as lamellar, dendritic etc, with the imposed thermodynamic conditions such as undercooling or supersaturation. These relations which have been derived for binary alloys will have to be modified to include the extra degree of freedom that allows for the choice of equilibrium compositions to depend on the diffusivity matrices for systems with greater than two components. This presents an exciting scope for future work.

ACKNOWLEDGEMENTS

The authors thank Department of Science and Technology for support through its Thematic Unit of Excellence program in computational materials science.

VI. APPENDIX

A. Thermodynamic information

The $\partial c/\partial \mu$ matrix was kept constant over both the phases and this is a thermodynamic parameter that was common to all calculations:

$$\frac{\partial c}{\partial \mu} = \begin{bmatrix} 1.1548 & 0.0535 \\ 0.0535 & 1.0025 \end{bmatrix} \quad (38)$$

B. Interfacial energy and width in phase field simulations

The interfacial energy and width are determined in all these simulations by using $\sigma = 1$ and $\epsilon = 4$ (which corresponds to about ten points in the interface for a grid resolution $dx=1$).

C. Non-dimensionalization

All values reported in this paper are non-dimensionalized. By choosing appropriate length, time and energy scales characterizing a particular system, we can retrieve dimensional quantities describing the growth behaviour of that system. The length l^* , time t^* and energy scales f^* are defined as,

$$f^* = \frac{1}{V_m} \left[\frac{\partial \mu_i}{\partial c_j} \right]_{max}, \quad (39)$$

$$l^* = \frac{\sigma}{f^*}, \quad (40)$$

$$t^* = \frac{l^{*2}}{[D_{ij}]_{max}}. \quad (41)$$

-
- [1] C. Zener, *Journal of Applied Physics* **20** (1949)
 - [2] F. C. Frank, *Proceedings of the Royal Society of London A: Mathematical, Physical and Engineering Sciences* **201**, 586 (1950), ISSN 0080-4630, <http://rspa.royalsocietypublishing.org/content/201/1067/586>
 - [3] F. S. Ham, *Journal of Physics and Chemistry of Solids* **6**, 335 (1958), ISSN 0022-3697, <http://www.sciencedirect.com/science/article/pii/0022369758900532>
 - [4] F. E. Bowman, *Trans. Am. Soc. Met* **36**, 61 (1946)
 - [5] H. Bhadeshia, *Progress in Materials Science* **29**, 321 (1985), ISSN 0079-6425, <http://www.sciencedirect.com/science/article/pii/0079642585900040>
 - [6] H. Aaronson and H. Domian, *AIME MET SOC TRANS* **236**, 781 (1966)
 - [7] J. B. Gilmour, G. R. Purdy, and J. S. Kirkaldy, *Metallurgical Transactions* **3**, 1455 (1972), ISSN 1543-1916, <http://dx.doi.org/10.1007/BF02643033>

- [8] M. Enomoto and H. I. Aaronson, Metallurgical Transactions A **18**, 1547 (1987), ISSN 1543-1940, <http://dx.doi.org/10.1007/BF02646138>
- [9] R. C. Sharma and J. S. Kirkaldy, Can. Met. Quart., 1973 **2**, 391 (1973)
- [10] R. C. Sharma, G. R. Purdy, and J. S. Kirkaldy, Metallurgical Transactions A **10**, 1129 (1979), ISSN 1543-1940, <http://dx.doi.org/10.1007/BF02811658>
- [11] D. E. Coates, Metallurgical Transactions **3**, 1203 (1972), ISSN 1543-1916, <http://dx.doi.org/10.1007/BF02642453>
- [12] D. E. Coates, Metallurgical Transactions **4**, 1077 (1973), ISSN 1543-1916, <http://dx.doi.org/10.1007/BF02645611>
- [13] J. P. Bourne, C. Atkinson, and R. C. Reed, Metallurgical and Materials Transactions A(1994)
- [14] A. Choudhury, Vol. Band 21 (KIT Scientific Publishing, 2012)
- [15] M. Plapp, Phys. Rev. E **84**, 031601 (2011)
- [16] A. Choudhury, M. Kellner, and B. Nestler, Current Opinion in Solid State and Materials Science **19**, 287 (2015)
- [17] Q. Chen, N. Ma, K. Wu, and Y. Wang, Scripta Materialia **50**, 471 (2004), ISSN 1359-6462, <http://www.sciencedirect.com/science/article/pii/S135964620300719X>
- [18] R. Qin, E. Wallach, and R. Thomson, Journal of Crystal Growth **279**, 163 (2005), ISSN 0022-0248, <http://www.sciencedirect.com/science/article/pii/S0022024805001624>
- [19] B. Böttger, J. Eiken, and I. Steinbach, Acta Materialia **54**, 2697 (2006), ISSN 1359-6454, <http://www.sciencedirect.com/science/article/pii/S1359645406001340>
- [20] I. Steinbach, B. Böttger, J. Eiken, N. Warnken, and S. G. Fries, Journal of Phase Equilibria and Diffusion **28**, 101 (2007), ISSN 1863-7345, <http://dx.doi.org/10.1007/s11669-006-9009-2>
- [21] N. Warnken, D. Ma, A. Drevermann, R. Reed, S. Fries, and I. Steinbach, Acta Materialia **57**, 5862 (2009), ISSN 1359-6454, <http://www.sciencedirect.com/science/article/pii/S1359645409005138>
- [22] B. Böttger, A. Carré, J. Eiken, G. J. Schmitz, and M. Apel, Transactions of the Indian Institute of Metals **62**, 299 (2010), ISSN 0975-1645, <http://dx.doi.org/10.1007/s12666-009-0046-5>
- [23] J. Lentz, A. Röttger, and W. Theisen, Acta Materialia **99**, 119 (2015), ISSN 1359-6454, <http://www.sciencedirect.com/science/article/pii/S135964541500508X>
- [24] D.-H. Yeon, P.-R. Cha, and J.-K. Yoon, Scripta Materialia **45**, 661 (2001), ISSN 1359-6462, <http://www.sciencedirect.com/science/article/pii/S1359646201010776>
- [25] A. Choudhury and B. Nestler, Phys.Rev.E **85**, 021602 (2011)
- [26] Strictly speaking, the composition relation in Eq. 21 is derived from a grand-potential density which is parabolic in μ . However, in this particular paper, we utilize a linearized form of the driving force in order to simplify its utilization in several non-linear equations in the sharp interface and analytical models. This just modifies the thermodynamic relation between the equilibrium diffusion potentials.
- [27] An important point to note here is that our analytical expressions are derived for a system where the precipitate phase grows into a supersaturated matrix which is infinite in extent. To ensure that our numerical calculations, in spite of being performed on finite systems, are representative of infinite systems, necessitate a few modifications. Phase field calculations are performed in a simulation box attached to the diffuse interface, which allows us to capture the scaling regime, otherwise impeded by the change in far-field compositions at the system boundaries due to growth, while sharp interface calculations are performed by expressing the governing equations in a reference frame attached to the interface. Thus, both our numerical techniques are attuned to capture growth in an infinite system.
- [28] Δc_B and Δc_C can vary with R during growth when the $\partial c/\partial \mu$ matrix is different for the matrix(α) and the precipitate (β) phases. For such a system, the scaling given by the constancy of λ_B^R and λ_C^R in Eq. 31 happens later in time, characterized by a slow change in $c_B(\eta_s)$ and $c_C(\eta_s)$ resulting in an asymptotic approach to a constant Δc_B and Δc_C .